Electronic Supplementary Information

High-Yield Bottom-Up Synthesis of 2D Metal Organic Frameworks and Their Derived Ultrathin Carbon Nanosheets for Energy Storage

Kuangmin Zhao,[ab] *Suqin Liu,*[*a] *Guanying Ye,*[ab] *Qingmeng Gan,*[ab] *Zhi Zhou,*[c] *and Zhen He*[*a]

[a]College of Chemistry and Chemical Engineering and [b]Innovation Base of Energy and Chemical Materials for Graduate Students Training, Central South University, Changsha, Hunan 410083, P.R. China.

[c]Science College of Hunan Agricultural University, Changsha, Hunan 410128, P.R. China.

*Corresponding authors: Zhen He (E-mail: zhenhe@csu.edu.cn) and Suqin Liu (E-mail: sqliu2003@126.com).

This file includes:

Fig. S1 to S16

Table S1

1. *The yields of the Zn(bim)(OAc) and UT-Zn(bim)(OAc).*

The theoretical weights of the Zn(bim)(OAc) and UT-Zn(bim)(OAc) synthesized according to the procedures described in the main text are 1.14 g. The real (experimental) weights of the Zn(bim)(OAc) and UT-Zn(bim)(OAc) obtained are about 0.9747 and 0.7433 g (as shown in Fig. S1), respectively. Therefore, the calculated yields of the Zn(bim)(OAc) and UT-Zn(bim)(OAc) are 87% and 65%, respectively.

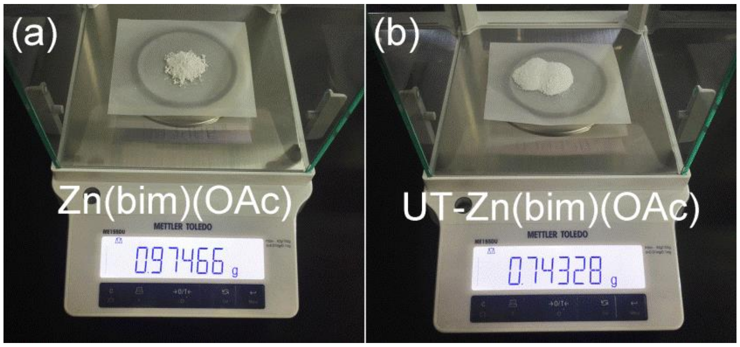

Fig. S1. Digital photographs showing the weights of (a) Zn(bim)(OAc) and (b) UT-Zn(bim)(OAc) synthesized following the procedures described in the main text.

2. *Preparation of the working electrodes and electrochemical measurements for supercapacitors.*

The working electrodes for supercapacitors were fabricated as follows. The sample, carbon black, and polytetrafluoroethene (PTFE 10 wt%) were mixed in ethanol with the weight ratios of 8:1:1, then the resultant mixture was rolled into a thin film. This film was pressed (under 8 MPa) onto a nickel foam and dried at 60 ^{o}C for 5 h. The mass loading of the sample on the prepared working electrode was about 5 mg cm^{-2}.

The cyclic voltammetry and galvanostatic charge/discharge tests were performed on a CHI 660D electrochemical workstation (Shanghai Chenhua Instrument Co., Ltd.). The specific capacitance, C_g (F g^{-1}), of the materials was calculated from the discharge curve based on eq. S1,

$$C_g = i\Delta t/\Delta V m \qquad \text{(S1)}$$

where C_g is the specific capacitance (F g^{-1}), i is the discharge current density (A g^{-1}), Δt is the discharge time (s), ΔV is the potential window of the discharge process (V), and m is the mass of the active material (g).

The electrochemical impedance spectroscopy (EIS) measurements were carried out using an EG&G Princeton Applied Research PARSTAT2273 potentiostat/galvanostat in the frequency range from 100 kHz to 0.01 Hz.

3. *Preparation of the working electrodes and electrochemical measurements for LIBs.*

The working electrodes were prepared by using a slurry coating method. In detail, the active material, superP carbon, and poly(vinylidene fluoride) in the weight ratios of 8:1:1 were first mixed using N-methyl-2-pyrrolidone as the solvent. Then, the slurry was cast onto a copper foil. After drying at 100 ^{o}C in vacuum for 10 h, the slurry-loaded copper foil was cut into disk electrodes (with a diameter of 8 mm) with a mass loading of about 2.0 mg cm^{-2}. The cells were assembled in an Ar-filled Braun Unilab glovebox and tested between 0 and 3 V vs. Li^+/Li on a LAND CT2001A testing system at 25 ^{o}C.

4. *XRD characterization of Zn(bim)(OAc).*

The XRD pattern of the Zn(bim)(OAc) was collected by using a Rigaku D/max 2500 instrument with the scan rate of 1^{o} min^{-1}. The result (Fig. S2) was indexed by using Materials

Studio and refined by Pawley fit ($P2_1/c$, a=10.817 Å, b=9.834 Å, c=8.817 Å, β=98.95°). The simulated data was plotted from the previously reported single crystal diffraction data (CSD, 754589). The packing diagram shows that the Zn(bim)(OAc) is a kind of layered MOFs constructed by the interactions of weak van de Waals force between the layers (Fig. S3).

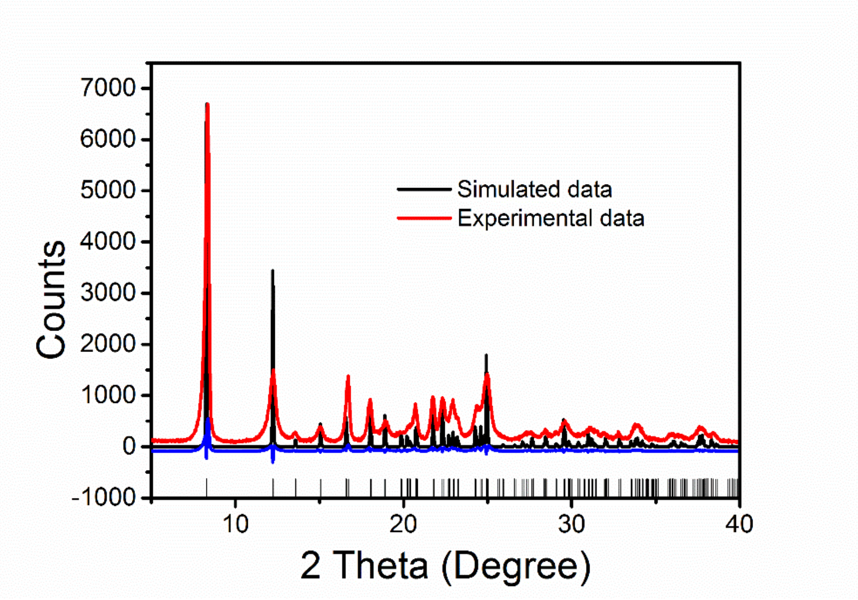

Fig. S2. Pawley fit of the XRD powder pattern of Zn(bim)(OAc).

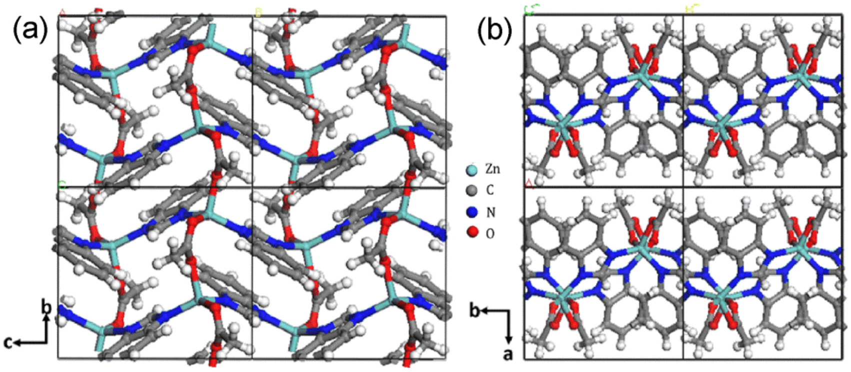

Fig. S3. Packing diagrams of Zn(bim)(OAc) along (a) [100] axis and (b) [001] axis showing the weak van der Waals interaction between two adjacent layers

5. *Elementral analysis and ICP-OES analysis of the as-synthesized Zn-bim based MOFs.*

The elemental analysis was used to determine the contents of C, N, O, and H. In the as-synthesized Zn-bim based MOFs, nitrogen could come only from bim whereas oxygen could only come from OAc, so the molar ratio of bim to OAc can be calculated according to the measured nitrogen and oxygen contents. The contents of Zn (wt%) in the synthesized Zn-bim based MOFs were calculated based on the ICP-OES measurements. Table S1 shows the chemical compositions of the as-synthesized $Zn_2(bim)_4$, Zn(bim)(OAc), and UT-Zn(bim)(OAc). The molar ratio of [Zn]:[bim] in the $Zn_2(bim)_4$ is about 1:2, whereas the molar ratios of [Zn]:[bim]:[OAc] in the Zn(bim)(OAc) and UT-Zn(bim)(OAc) are about 1:1:1. The oxygen content in the UT-Zn(bim)(OAc) (13.71 wt%) is slightly higher than that in the Zn(bim)(OAc) (13.10 wt%). Besides, the oxygen content increases with the increase of the amount of gluconate added during the synthetic processes (e.g., the oxygen content is about 14.02 wt% in the $Zn(bim)(OAc)_{1000mg}$), indicating that a small amount of the gluconate might coordinate with the Zn ions on the surfaces of the Zn(bim)(OAc) crystals.

Table S1. Elemental analysis of the $Zn_2(bim)_4$, Zn(bim)(OAc), UT-Zn(bim)(OAc), and $Zn(bim)(OAc)_{1000mg}$

	Zn (wt%)	**C (wt%)**	**N (wt%)**	**O (wt%)**	**H (wt%)**
$Zn_2(bim)_4$	21.80	56.24	18.82	0.02	3.12
calc.	21.74	56.19	18.73	0.00	3.34
Zn(bim)(OAc)	26.67	45.02	11.84	13.10	3.37

calc.	27.09	44.74	11.60	13.26	3.31
UT-Zn(bim)(OAc)	26.02	45.47	11.42	13.71	3.38
calc.	27.09	44.74	11.60	13.26	3.31
Zn(bim)(OAc)$_{\mathbf{1000mg}}$	25.32	46.01	11.24	14.02	3.41
Calc.	27.09	44.74	11.60	13.26	3.31

6. *SEM study of $Zn_2(bim)_4$ and Zn(bim)(OAc)*

The SEM images of $Zn_2(bim)_4$ and Zn(bim)(OAc) (Fig. S4) both show the bulk-like morphology, which is coincident with the hypothetical morphologies purposed in Scheme 1 in the main text.

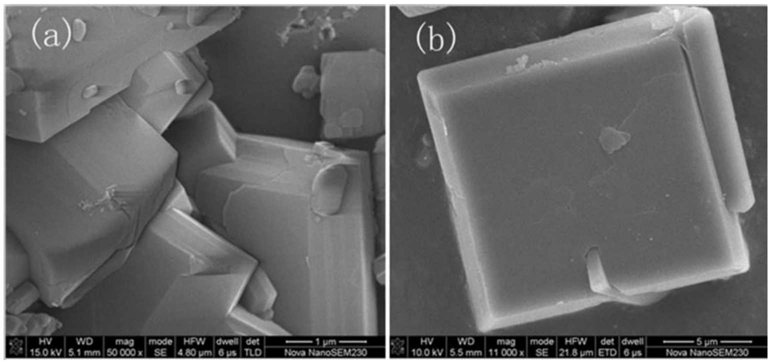

Fig. S4. SEM images of (a) $Zn_2(bim)_4$ and (b) Zn(bim)(OAc).

7. *SEM studies of the Zn(bim)(OAc) synthesized with hydrophobic long-chain acids.*

In order to select the suitable assistant reagent for the synthesis of the Zn(bim)(OAc) nanosheets, several long-chain carboxylates (i.e., sodium butyrate and sodium laurate) have been tested. Unfortunately, no Zn(bim)(OAc) prepared with hydrophobic long-chain carboxylates achieves the ultrathin nanosheet morphology (Fig. S5). The precipitation occurs when sodium butyrate or sodium laurate is added to the $Zn(NO_3)_2$ solution (Fig. S5a). The Zn(bim)(OAc) synthesized using these inhomogeneous solutions doesn't show a nanosheet morphology (Fig. S5b and S5c). When a hydrophilic long-chain carboxylate (i.e., sodium gluconate in our case) is used as the assistant reagent to coordinate with Zn^{2+}, a homogeneous solution forms (Fig. S5a), and the UT-Zn(bim)(OAc) nanosheets with a thickness of about 5 nm have been successfully obtained by using this gluconate-assisted (GA) method as we present in the main text.

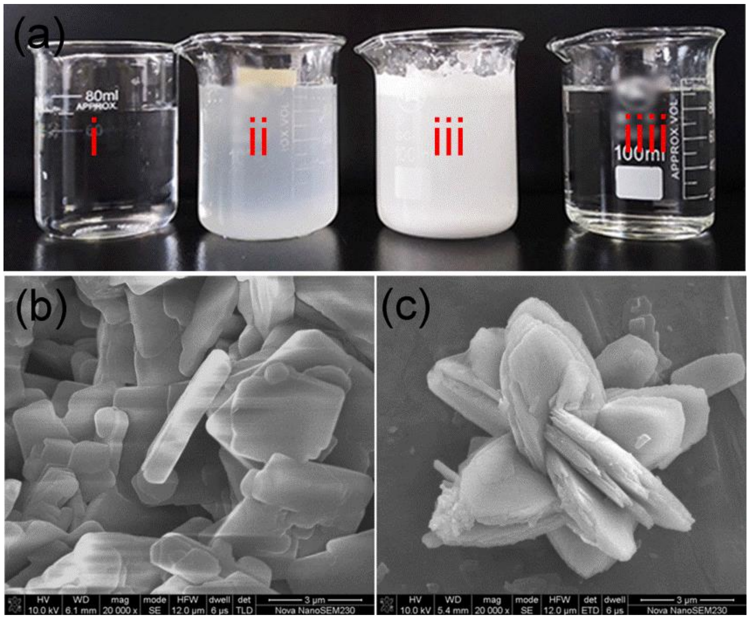

Fig. S5. (a) Digital photos of the $Zn(NO_3)_2$ solutions mixed with (i) none, (ii) sodium butyrate, (iii) sodium laurate, and (iiii) sodium gluconate. SEM images of Zn(bim)(OAc) prepared with (b) sodium butyrate and (c) sodium laurate.

8. AFM study of UT-Zn(bim)(OAc)

As shown in Fig. S6, the thickness and size (i.e., lateral diameter) of the UT-Zn(bim)(OAc) based on 70 pieces of the UT-Zn(bim)(OAc) nanosheets are measured by AFM and statistically analyzed by using the Nanoscope analysis software. The measured thicknesses of the UT-Zn(bim)(OAc) nanosheets are in the range of about 1.0 to 6.5 nm with most of the nanosheets around 5 nm (Fig. S6b). Meanwhile, the statistical analysis shows that most of the measured UT-Zn(bim)(OAc) nanosheets have a size of about 2.6 μm (Fig. S6c). For the size measurements, the size of a nanosheet is equal to the diameter of a circle with the same area as the measured nanosheet.

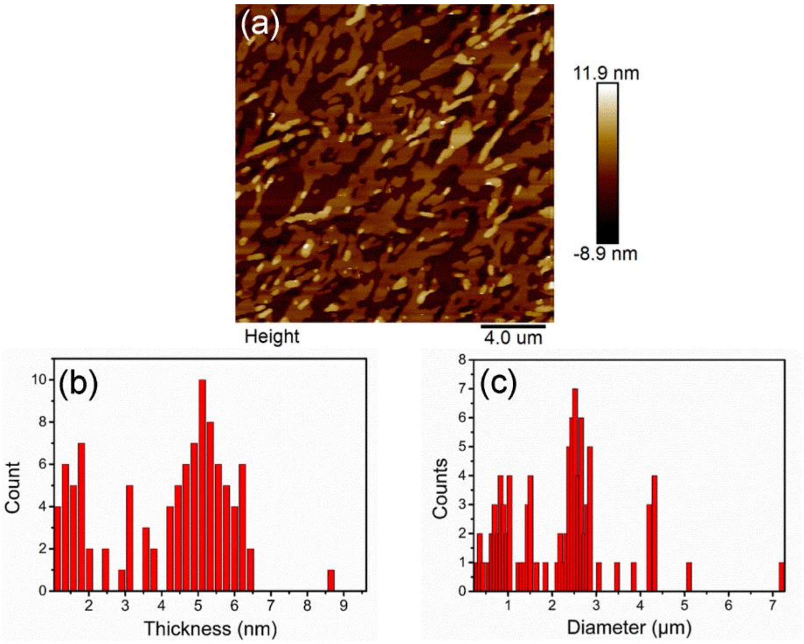

Fig. S6. (a) AFM image of the UT-Zn(bim)(OAc) nanosheets and the calculated (b) thickness distribution and (c) size distribution of the UT-Zn(bim)(OAc) nanosheets.

9. UV-vis analysis on the role of gluconate in the synthesis of UT-Zn(bim)(OAc).

For the UV-vis analysis, $Zn(NO_3)_2$ and gluconate were dissolved in ethanol/water(1:1 v:v) solutions, respectively. Then, the $Zn(NO_3)_2$ and gluconate solutions were mixed with the molar ratios of 1:2 and 1:4, resulting in two solutions with different amount of uncoordinated and coordinated $–COO^-$. The UV-vis spectra of the solutions containing different amounts of coordinated and uncoordinated $–COO^-$ are shown in Fig. S7. The band around 212 nm is the characteristic peak (n→π*) of the uncoordinated $–COO^-$.[S1] This peak shows blue shifts (from 212 to 208 nm in the $Zn(NO_3)_2$:Gluconate=1:4 and from 212 to 205 nm in the

$Zn(NO_3)_2$:Gluconate=1:2 solution) as the ratio of $Zn(NO_3)_2$ in the solution increases, indicating that the gluconate has partially coordinated with Zn^{2+}. When the benzimidazole is added into the $Zn(NO_3)_2$:Gluconate=1:2 solution, the characteristic peak of $–COO^-$ shows slightly red shift (from 205 to 208 nm), indicating that the coordinated gluconate has been released from the Zn-gluconate complexes.

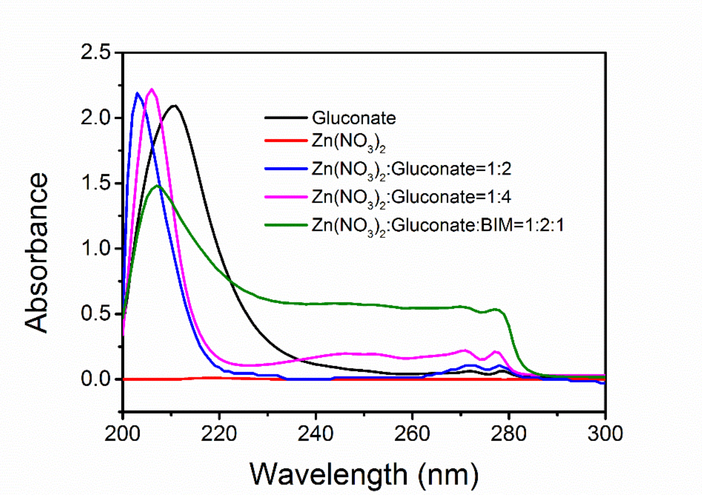

Fig. S7. UV-Vis absorption spectra of gluconate, $Zn(NO_3)_2$, and $Zn(NO_3)_2$ mixed with different amounts of gluconate in ethanol/water(1:1) solution. The spectrum of the $Zn(NO_3)_2$ solution is used as the reference to remove the absorption peak of NO_3^-.

10. N_2 adsorption-desorption analysis of the Zn(bim)(OAc) and UT-Zn(bim)(OAc).

The external surface areas or statistical thickness surface areas (STSA) of the Zn(bim)(OAc) and UT-Zn(bim)(OAc) are calculated from their N_2 adsorption-desorption isotherms (Fig. S8). The statistical thickness (t) was calculated based on the following equation,

$$t = (13.99/(0.034-\log(P/P_0)))\text{^}0.5$$

and the STSA was calculated from the V-t plot by using the following equation,

$$\mathrm{STSA} = \mathrm{M} \times 15.47$$

where M is the linear fitting slope of the V-*t* plot and 15.47 is the volumetric conversion constant of nitrogen gas to liquid nitrogen.

As shown in Fig. S8, the STSAs of the UT-Zn(bim)(OAc) and Zn(bim)(OAc) calculated from their V-*t* plots (Fig. S8b) are 369.42 and 53.83 m^2 g^{-1}, respectively. These results show that the UT-Zn(bim)(OAc) owns a much higher exposed external surface area compared to the Zn(bim)(OAc), which suggests that the thickness of the UT-Zn(bim)(OAc) sheets is much smaller than that of the Zn(bim)(OAc).

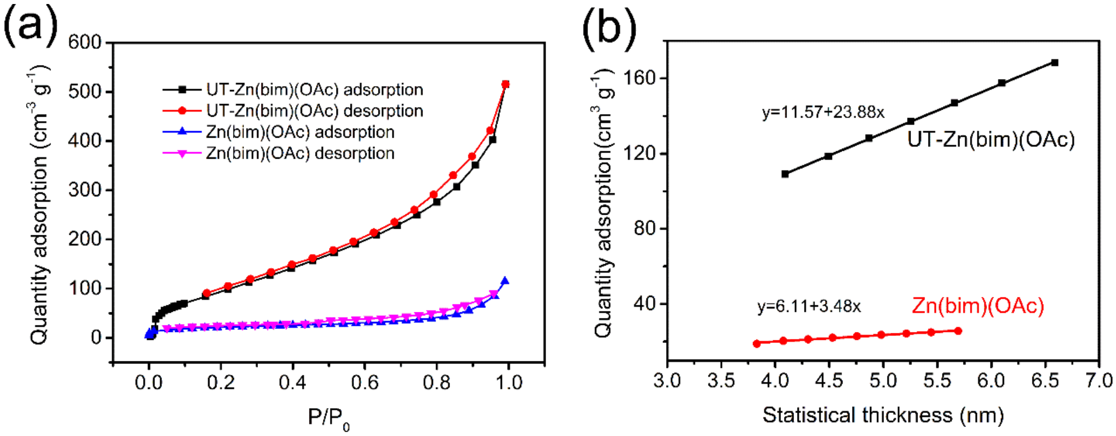

Fig. S8. (a) N_2 adsorption-desorption isotherms. (b) V-*t* plots of the UT-Zn(bim)(OAc) and Zn(bim)(OAc).

11. SEM study of CNC, L-CNC, and UT-CNC.

The morphologies of CNC and L-CNC (Fig. S9) are similar to those of their corresponding MOF precursors (i.e., $Zn_2(bim)_4$ and Zn(bim)(OAc) as shown in Fig. S4). However, the L-CNC shows a more obvious layered structure compared to the CNC, which might be attributed to the larger interlayer distance of the corresponding MOF precursor (Scheme 1 in main text).

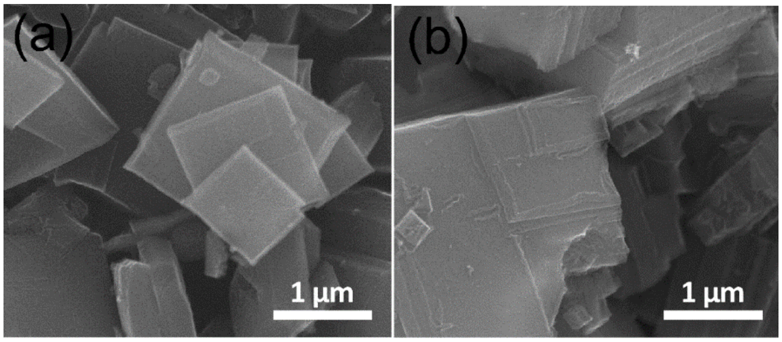

Fig. S9. SEM images of (a) CNC and (b) L-CNC.

The SEM images of the UT-CNS samples prepared with different amounts of sodium gluconate are presented in Fig. S10. All the UT-CNS samples exhibit a nanosheet morphology, indicating that the gluconate is an effective additive for the synthesis of nanosheets.

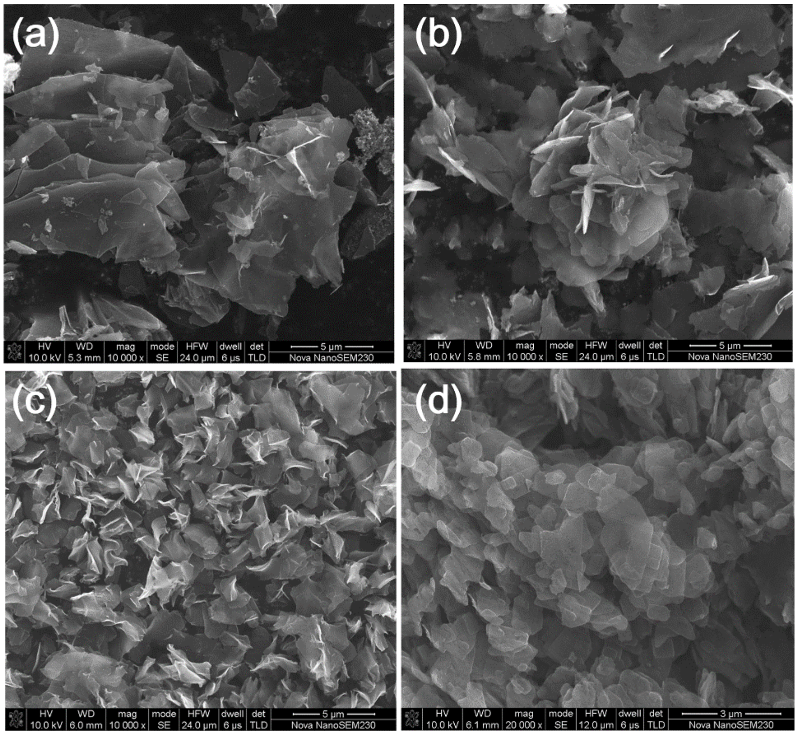

Fig. S10. SEM images of the UT-CNS prepared with different amounts of sodium gluconate: (a) 100 mg, (b) 200 mg, (c) 250 mg, and (d) 500 mg.

12. TEM study of UT-CNS

A FEI Titan G2 60-300 TEM was used to analyze the porosity and elemental distribution of the UT-CNS. The high angle annular dark field (HAADF) image (Fig. S11) exhibits the high porosity of the UT-CNS, and EDS mapping analysis reveals uniform distributions of C and N in the UT-CNS. The bright areas in the HAADF are the C or N, whereas the dark areas are the pores.

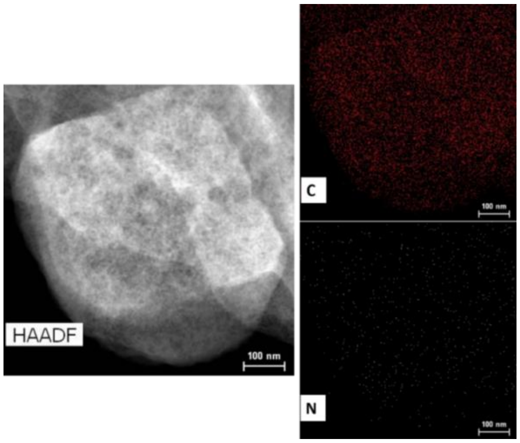

Fig. S11. HAADF image and EDS elemental mapping analysis of the UT-CNS.

13. AFM analysis of UT-CNS

The UT-CNS was further investigated by AFM (Fig. S12). The thicknesses and sizes of 57 pieces of UT-CNS (in Fig. S12a) were measured and statistically analyzed, as shown in Fig. S12b and S12c. The average thickness of the UT-CNS based on the 57 pieces of the UT-CNS (in Fig. S12a) is estimated to be around 2.5±0.8 nm with a thickness distribution of 1.8 to 3.3 nm. Fig. S12b shows the examples of the thickness measurements. For the size measurements, the size of a UT-CNS nanosheet is equal to the diameter of a circle with the same area as the measured nanosheet. Based on the measurements on the 57 pieces of UT-CNS, the average size of the UT-CNS is around 2.5±1.1 μm (Fig. S12c).

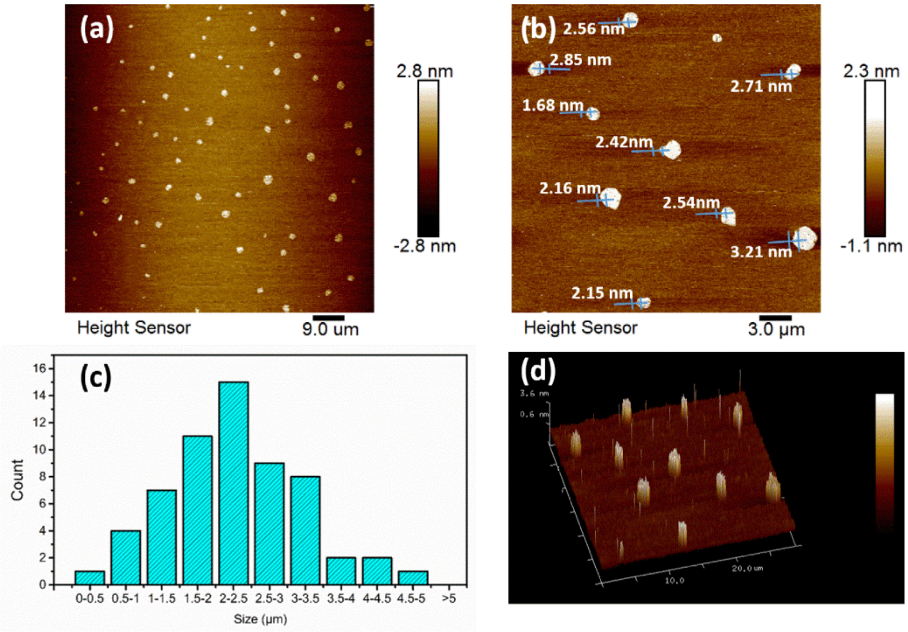

Fig. S12. (a, b) AFM images of UT-CNS with different scan ranges. (c) Statistical analysis of the size distribution of the UT-CNS. (d) 3D view of the AFM image of UT-CNS.

14. XPS analysis of the CNC, L-CNC, and UT-CNS.

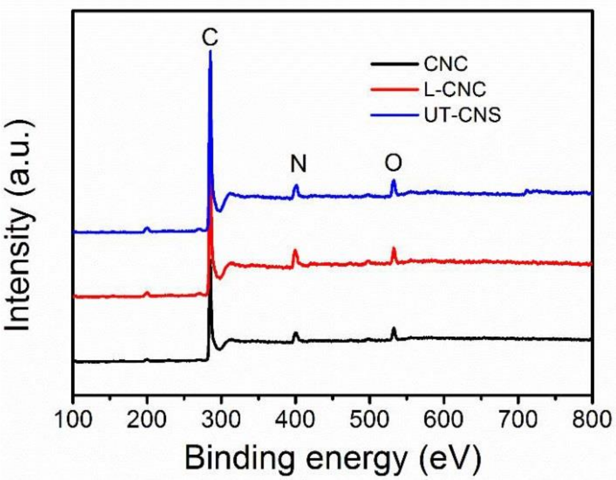

Fig. S13. XPS survey spectra of the UT-CNS (blue curve), CNC (black curve), and L-CNC (red curve). The XPS survey scans show that the main elements on the surfaces of these three samples are carbon, oxygen, and nitrogen, and the nature of the chemical bonding in these three samples varies only slightly.

15. Effects of gluconate on the morphology and electrochemical performance of the UT-CNS.

The gluconate plays an important role in the synthesis of the UT-Zn(bim)(OAc) nanosheet, as discussed in the main text (Scheme 1). The amount of the gluconate used during the synthesis would affect the morphologies of the Zn(bim)(OAc) MOF precursor as well as its carbonized product (i.e., the CNS). The SEM images of the CNS samples derived from the Zn(bim)(OAc) MOF precursors synthesized by using different amounts of gluconate (from 0 to 2000 mg) are shown in Fig. S14. Basically, the thickness of the CNS decreases as the amount of gluconate used in the synthesis of the MOF precursor increases. As discussed in the main text, only a small amount of gluconate coordinate with the Zn ions on the surfaces of the Zn(bim)(OAc) crystals. Therefore, as the amount of gluconate used in the synthesis of the MOF precursor increases,

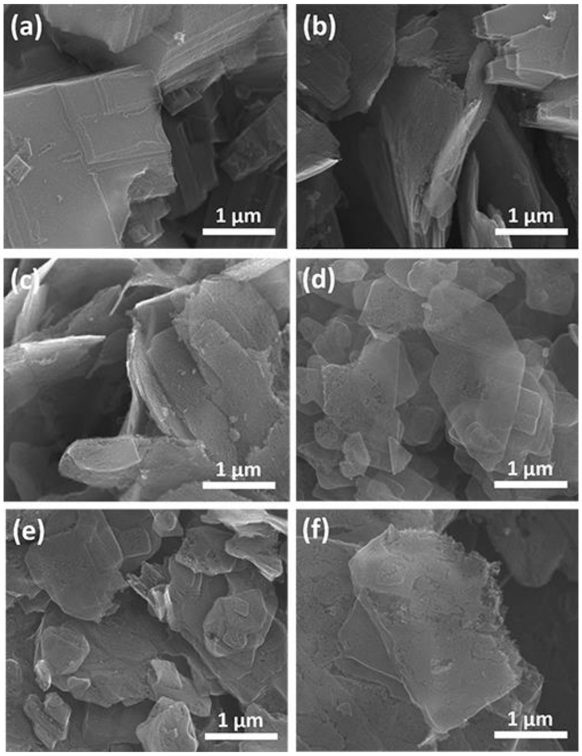

Fig. S14. SEM images and specific capacitance of UT-CNS prepared with different amounts of sodium gluconate, (a) L-CNC 0 mg, (b) 50 mg, (c) 200 mg, (d) 500 mg, (e) 1000 mg, and (f) 2000 mg.

more and more carbon in the final carbonized product is derived from the excess gluconate (i.e., the uncoordinated gluconate). However, the carbon derived directly from the gluconate might not possess the capacity performance as good as the MOF-derived carbon. Based on our measurements, the UT-CNS derived from the UT-Zn(bim)(OAc) nanosheet synthesized by using 200 mg sodium gluconate shows the best performance for the SC applications (Fig. S15).

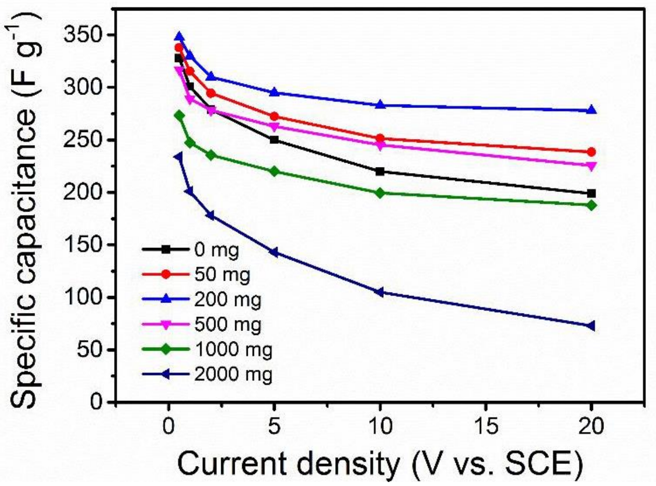

Fig. S15. Capacity performance of the UT-CNS prepared with different amounts of sodium gluconate.

16. Ion Diffusion of the CNC, L-CNC, and UT-CNS electrodes.

The supercapacitor performance related to the ion diffusion of the electrode was studied by using the EIS technique to correlate the electrolyte ion transport limitations within the microstructures of the prepared electrodes. The Nyquist plot of the UT-CNS electrode features a larger phase angle compared to those of the CNC and L-CNC electrodes at low frequencies (Fig. S16). This indicates that the UT-CNS electrode possesses a capacitive behavior closer to the ideal EDLC and a faster ion diffusion ability compared to the CNC and L-CNC electrodes.[S2] The enhanced performance of the UT-CNS electrode is mainly due to the unique porous 2D structure of the

UT-CNS. which could significantly shorten the diffusion distance of the electrolyte ions. For the diffusion of ions, it is well known that the diffusion time (t) is greatly depended on the diffusion distance (L) and diffusion coefficient (D), which can be expressed by the following eq. S2.[S3]

$$t = L^2/D \qquad \text{(S2)}$$

When the diffusion length is shortened by the 2D structure of the UT-CNS, the diffusion time of ions in the UT-CNS electrode is significantly shortened and the reaction kinetic is enhanced. The enhanced diffusion kinetic, excellent conductivity, and large surface area ensure the superior supercapacitive performance of UT-CNS.

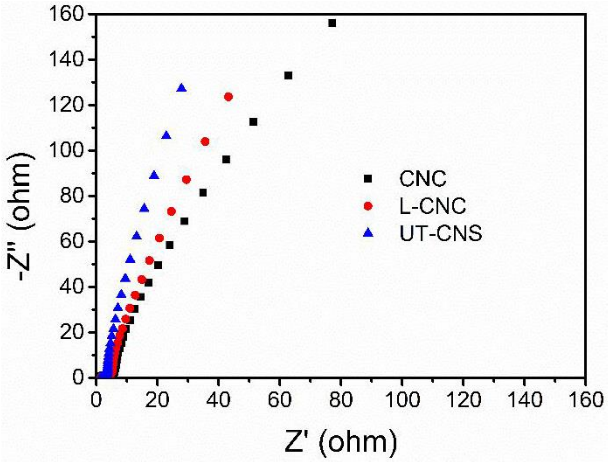

Fig. S16. EIS spectra of the UT-CNS, L-CNC, and CNC electrodes.

Supporting References

(S1) Y.-Z. Zheng, M.-L. Tong, W.-X. Zhang, X.-M. Chen, *Angew.Chem. Int. Ed.* 2006**, 118**, 6458-6462.

(S2) G.-P. Hao, A.-H. Lu, W. Dong, Z.-Y. Jin, X.-Q. Zhang, J.-T. Zhang, W.-C. Li, *Adv. Energy Mater.* 2013**, 3**, 1421-1427.

(S3) X. Zhuang, F. Zhang, D. Wu, X. Feng, *Adv. Mater.* 2014, **26**, 3081-3086.